

# Influence of growth temperature and silver to sulfur molar ratios on optical, electrical and thermoelectrical properties of nanostructured Ag<sub>2</sub>S thin films

M. Adelifard<sup>1</sup> · R. Torkamani<sup>1</sup>

Received: 16 April 2015 / Accepted: 21 June 2015 / Published online: 1 July 2015  
© Springer Science+Business Media New York 2015

**Abstract** Silver sulfide (Ag<sub>2</sub>S) thin films have been deposited onto glass substrates using spray pyrolysis technique. The substrate temperature (260–310 °C) and also Ag to S molar ratio (0.33 and 0.43) dependent structural, morphological, optical, electrical and thermoelectrical properties of samples have been studied. The X-ray diffraction studies showed that the samples have single acanthite ( $\alpha$ -Ag<sub>2</sub>S) phase with monoclinic structure and preferred orientation change from ( $\bar{1}12$ ) to ( $\bar{1}03$ ) plan with increasing sulfur content. SEM and AFM analyses revealed a compact surface morphology with slightly rough surface. Optical measurements showed a relatively high absorption coefficient ( $\sim 5 \times 10^4$ – $6 \times 10^5$  cm<sup>-1</sup>) in the visible range, with an effective optical band gap of  $\sim 2.01$ – $2.23$  eV. The electrical studies showed that all these samples have an n-type conductivity and the free electron density increases with increasing the substrate temperature, in agreement with the reflectance spectra of the layers. The thermoelectric measurements revealed that the maximum Seebeck coefficient of  $-198$   $\mu$ V/K (at T = 400 K) was obtained for Ag<sub>2</sub>S (Ag:S = 0.33 at.%) film at substrate temperature of 310 °C.

## 1 Introduction

The optical and electrical properties of transition metal chalcogenides such as sulfides, selenides and tellurides make these semiconductors promising candidate for their various applications in science and technology. Ag<sub>2</sub>S is

such a material which has several applications in the fields such as IR detectors, photoconductors, photovoltaic cells, electrochemical storage cells [1–5], etc. Silver sulfide presents two main allotropic crystallographic modifications. The first is monoclinic modification acanthite ( $\alpha$ -Ag<sub>2</sub>S) and the second ( $\beta$ -Ag<sub>2</sub>S) is cubic modification argentite [1, 3]. In contrast to acanthite, that shows a semiconducting behavior, argentite is reported to have quasi-metallic behavior, which is not interesting for semiconductor application [3]. Silver sulfide presents a high absorption coefficient ( $>10^4$  cm<sup>-1</sup>) and a narrow band gap energy above 0.6–1 eV [6] for indirect transition and about 2–2.3 eV for direct transition in the acanthite phase [1–4, 6, 7].

The reported synthesis methods for silver sulfide structures include several routes such as chemical bath deposition (CBD) [2], spray pyrolysis deposition (SPD) [1, 5], successive ionic layer absorption and reaction (SILAR) [2, 8], sequential thermal evaporation [4], sol–gel and ion implantation techniques [3], molecular beam epitaxy (MBE) [9] and gamma irradiation [10]. Among all these techniques, SPD is the promising one, because of its simplicity and the facility for cost effective large area deposition, with no need of any sophisticated instrumentation.

The composition, morphology, optical, electrical and thermoelectrical properties of Ag<sub>2</sub>S thin films, deposited by spray pyrolysis, can be tailored by changing the composition of precursors' solution (Ag:S molar ratio, type of solvent) and deposition parameters, especially the substrate temperature. Sahraoui et al. [1], investigated the structural and optical properties of Ag<sub>2</sub>S, depending on the composition of precursor solution (aqueous solution of AgCl and thiourea with the concentration  $x = [\text{CS}(\text{NH}_2)_2]/[\text{AgCl}] = 5, 7$  and 9) at two different temperatures of 200 and 250 °C. Although there have been little theoretical and

✉ M. Adelifard  
adelifard@du.ac.ir

<sup>1</sup> School of Physics, Damghan University, Damghan, Iran

experimental studies on the transport phenomena, electrical, and thermoelectrical properties of silver sulfide crystals [11–13], the basis of our knowledge, no real authentic information was available relative to nature of electrical-thermoelectrical of Ag<sub>2</sub>S polycrystalline thin films deposited by chemical spray pyrolysis technique.

In this paper, we have achieved to this goal using aqueous solutions of CH<sub>3</sub>CO<sub>2</sub>Ag and thiourea with different Ag:S molar ratios at various temperatures to assess the potential of these thin films as optoelectronic materials. In this study, we have investigated the corresponding samples from various viewpoints, including structural (crystallinity and surface morphology), optical (UV–Vis–Near IR transmittance/reflectance spectra), electrical (carrier density and resistivity) and thermoelectrical properties.

## 2 Experimental description

Silver sulfide thin films were deposited onto glass substrate by spray pyrolysis method. In order to prepare the basis spray solution for any sample, 0.04 M (0.667 g) of silver acetate (CH<sub>3</sub>CO<sub>2</sub>Ag) was added to 100 ml double distilled water. Then thiourea [CS(NH<sub>2</sub>)<sub>2</sub>] as the source for sulfur with two various Ag to S molar ratios of 0.33 [Ag:S = 1:3; for samples S1–S3 in group (a)], and 0.43 [Ag:S = 1:2.28; for samples S4–S6 in group (b)] was dissolved into the basis solution. The calculation of the amount of CS(NH<sub>2</sub>)<sub>2</sub> (? g) with Ag/S = 0.33 at.% and Ag/S = 0.43 at.% in solution is described in the following:

$$[\text{Ag} = 0.04 \text{ M}]/[\text{S}] = 0.33 \rightarrow [\text{S}] = 0.121 \text{ M} \tag{1}$$

$$0.121(\text{mol}/1000 \text{ ml}) \times 100 \text{ ml} \\ \times (\text{Molar Mass of CS(NH}_2)_2 = 76.12 \text{ gmol}^{-1}) \\ = 0.921 \text{ g} \tag{2}$$

$$[\text{Ag} = 0.04 \text{ M}]/[\text{S}] = 0.43 \rightarrow [\text{S}] = 0.091 \text{ M} \tag{3}$$

$$0.091(\text{mol}/1000 \text{ ml}) \times 100 \text{ ml} \\ \times (\text{Molar Mass of CS(NH}_2)_2 = 76.12 \text{ gmol}^{-1}) \\ = 0.692 \text{ g} \tag{4}$$

To enhance the solubility of thiourea, a few drops of acetic acid was also added to the solution. The final solution was stirred for 30 min. Before spraying the solution, the substrate temperature (T<sub>S</sub>) was varied from 260 to 285 and 310 °C with an accuracy of ±5 °C using a digital temperature controller for both options. Other deposition parameters such as spray deposition rate (ml/min), spray solution volume and the pressure of the carrier gas were reported in Table 1.

An X-ray diffractometer (D8 Advance Bruker) was used to record X-ray diffraction (XRD) patterns using Cu-K<sub>α</sub> radiation (λ = 0.15406 nm) spectra in the 2θ range 10°–

70°. Spectral transmittance and reflectance were recorded in the wavelength range 300–1100 nm by a Shimadzu UV1800 spectrophotometer. The surface morphology were investigated by using an Atomic Force Microscope (AFM; DME, model: 95-50-E) and field emission scanning electron microscope (FESEM; Hitachi, model: S-4160).

The film thickness was measured using a Taly step profilometer (roughness detector with a stylus-Taylor Hobson model). Taly profile (a dedicated software package designed for use with laboratory instruments) has complete laboratory analysis functions such as: roughness parameters and Step height measurement etc.; and the information can be displayed graphically and numerically. By step height measurement between coated glass and uncoated part of glass we could determine the thickness of the studied samples with a precision of about 10 nm.

Electrical resistivity and Hall effect data (magnetic field strength = 200 mT) of the samples were measured in the Van der Pauw configuration [14]. Finally by applying a temperature gradient between the two ends of the samples, the thermoelectric electromotive force (emf) of the prepared films was measured, and then the Seebeck coefficients were determined by calculating the slope of the thermoelectric emf versus temperature difference.

## 3 Results and discussion

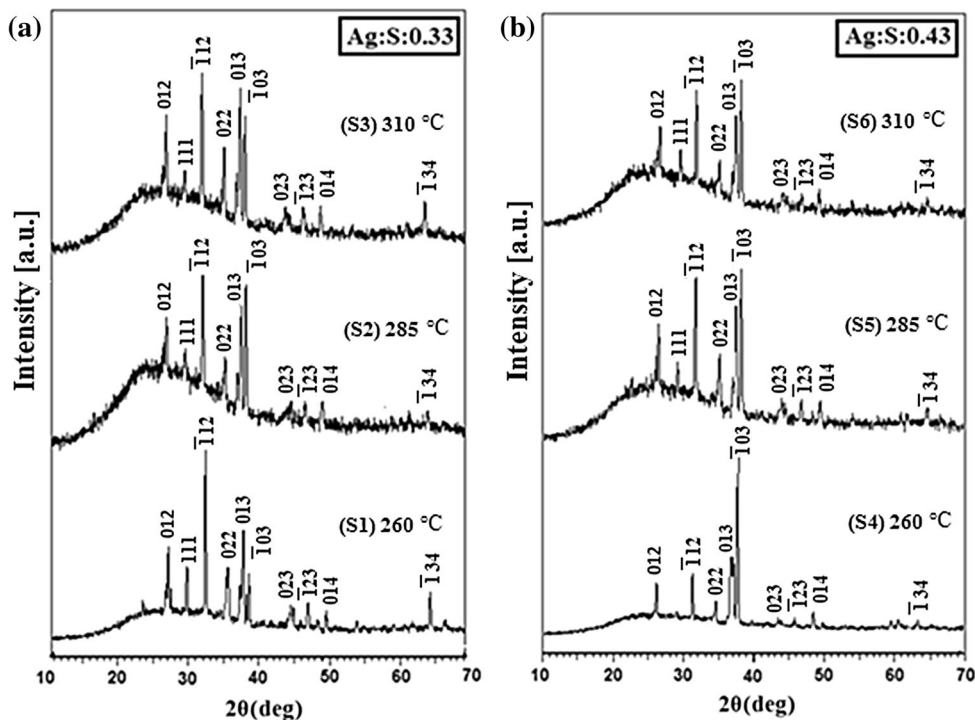
### 3.1 Structural characterization

Figure 1 presents the XRD patterns of Ag<sub>2</sub>S thin films synthesized with two different Ag/S molar ratios (0.33 and 0.43), as well as at various substrate temperatures between 260 and 310 °C. The data analysis show the single acanthite phase with monoclinic crystal structure, with (012), (111), (1̄12), (022), (013), (1̄03), (1̄23) and (014) planes in all the studied samples [1–6]. Ag<sub>2</sub>S thin films prepared from silver acetate (CH<sub>3</sub>CO<sub>2</sub>Ag) showed an interesting property in XRD analysis. Samples S1–S3 prepared using Ag/S molar ratio of 0.33 at various substrate temperatures exhibited a good crystalline property depicted in Fig. 1a. It should be mentioned that When the molarity increases (Ag/S = 0.43), the intensity of (1̄12) peak decreases and the preferred orientation change from (1̄12) to (1̄03) plan in S4–S6 samples (Fig. 1b). The modification in the preferential crystallite direction could be attributed to the change of the preparation conditions. Also, with increasing the substrate temperature from 260 to 310 °C, not only the intensity of peak correspond to (013) increases in two groups (a) and (b), but also (1̄12) peak first reduces from S1 to S2 sample and then increases in sample S3, so that in substrate temperature of 285 °C (S2), the (1̄03) peak has

**Table 1** The chemical deposition parameters for Ag<sub>2</sub>S thin films by spray pyrolysis technique

Sample	T <sub>s</sub> (°C)	Ag:S	Spray volume (ml)	Spray rate (ml/min)	P (bar)
Group (a) (Ag:S = 0.33)					
S1	260	1:3 = 0.33	100	10	3
S2	285	1:3	100	10	3
S3	310	1:3	100	10	3
Group (b) (Ag:S = 0.43)					
S4	260	1:2.28 = 0.43	100	10	3
S5	285	1:2.28	100	10	3
S6	310	1:2.28	100	10	3

**Fig. 1** X-ray diffraction patterns of Ag<sub>2</sub>S thin films deposited at various substrate temperatures for group (a) and (b) samples



been dominated. Also, the  $d_{hkl}$  experimental values, for samples are compared with data (from JCPDS card No.: 14-0072); and are found to be in good agreement with the standard values as shown in Table 2.

The crystallites average sizes ( $D$ ) of 30–35 nm have been determined (see Table 3) using the well-known Scherrer equation:

$$D = \frac{0.9\lambda}{\beta \cos \theta} \quad (5)$$

where  $\lambda$  is the X-ray wavelength,  $\beta$  is the full-width at half-maximum of the main peak and  $\theta$  is the Bragg angle. The variation of the crystallite size has major influence on optical and electrical properties of the samples, as described in the following.

### 3.2 Morphological studies

In order to study the surface morphology, the produced films were examined by FESEM, Fig. 2. As can be seen, there exists difference in the FESEM images of these films. The differences in surface morphology of the Ag<sub>2</sub>S films in two groups (a) and (b) with different Sulfur content can be explained as a consequence of difference in the preferred orientation of grains or crystallites corresponding to ( $\bar{1}12$ ) and ( $\bar{1}03$ ) planes, respectively; with predominant influence in the growth, and different deposition temperature, with strong influence in the nucleation step. The samples except S2 and S6 show a smooth, compact and crack-free morphology. The existence of some holes on the surfaces of S2 and S6 samples are probably due to very small droplets

**Table 2** Comparison of observed “d” values, obtained from XRD data of samples prepared at various substrate temperature, with the standard “d” values, from ICSD card No. 044507

Sample	S1	S2	S3	S4	S5	S6	Ag <sub>2</sub> S (JCPDC-14-0072)	
							(hkl)	Standard d <sub>hkl</sub> values
2θ	d <sub>hkl</sub> (Å) (realized)							
26.56	3.355	3.358	3.355	3.356	3.353	3.354	(012)	3.383
29.27	3.050	3.056	3.054	3.047	3.055	3.053	(111)	3.080
31.79	2.814	2.818	2.811	2.815	2.813	2.815	( $\bar{1}$ 12)	2.836
34.98	2.564	2.564	2.566	2.564	2.561	2.563	(022)	2.583
37.35	2.407	2.410	2.409	2.409	2.409	2.411	(013)	2.421
38.01	2.367	2.368	2.367	2.366	2.367	2.366	( $\bar{1}$ 03)	2.383
44.02	2.056	2.041	2.056	2.061	2.060	2.071	(023)	2.072
46.47	1.954	1.955	1.954	1.955	1.955	1.954	( $\bar{1}$ 23)	1.963
48.94	1.861	1.862	1.861	1.857	1.861	1.859	(014)	1.866
64.07	1.452	1.455	1.451	1.452	1.450	1.454	( $\bar{1}$ 34)	1.459

**Table 3** The crystallite size and roughness of the studied films

Sample	Substrate temperature (°C)	D (nm) (hkl)	Roughness (nm)
Group (a) (Ag:S = 0.33)			
S1	260	32.76 ( $\bar{1}$ 12)	33
S2	285	32.65 ( $\bar{1}$ 03)	31.9
S3	310	31.26 ( $\bar{1}$ 12)	33.1
Group (b) (Ag:S = 0.43)			
S4	260	33.06 ( $\bar{1}$ 03)	37.9
S5	285	35.12 ( $\bar{1}$ 03)	43.6
S6	310	31.08 ( $\bar{1}$ 03)	39.3

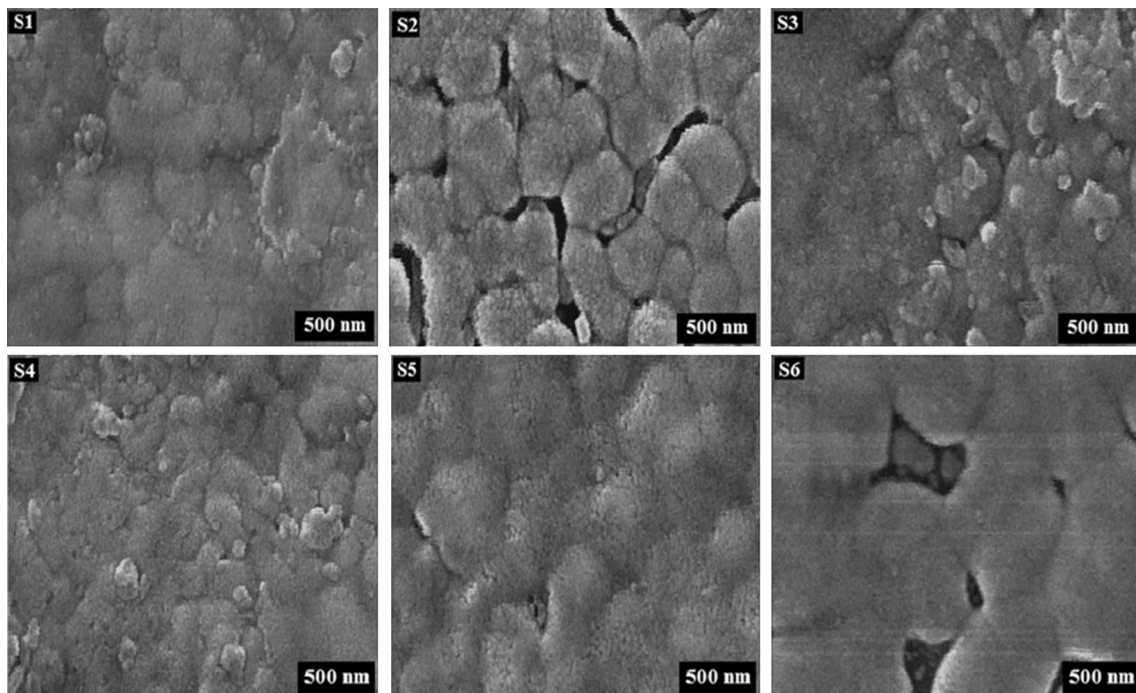


**Fig. 2** FESEM images of Ag<sub>2</sub>S thin films

resulting from the spray pyrolysis technique, which vaporize above the glass substrates and condense as some voids on the surface. Also, it can be seen that, Sample S2 is covered with compact globular structures composed of hierarchical spherical particles. The average diameter of the globules is less than 500 nm and the diameter of the spherical particles, by which the globules are made, are around 20–40 nm. These particle sizes are fairly well matched with those obtained by XRD analysis.

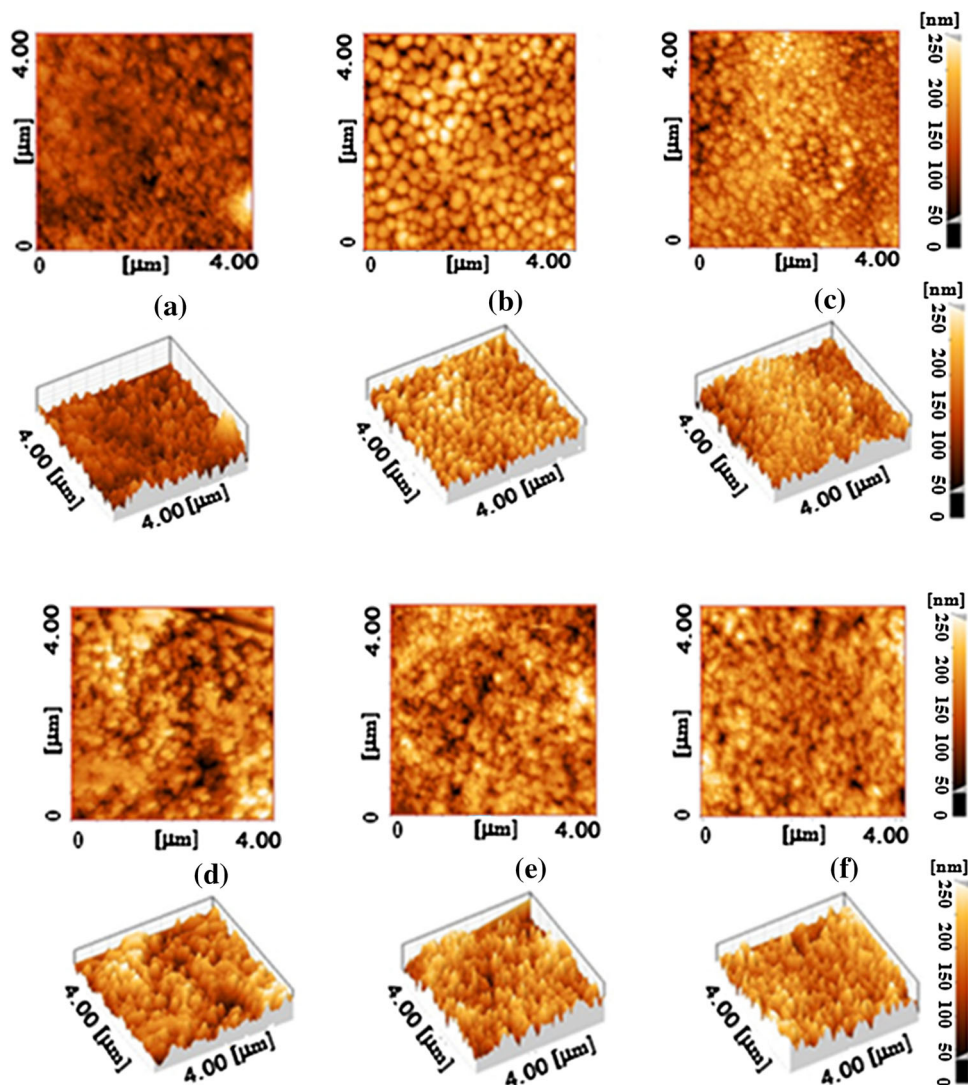
Two dimensional and three dimensional micrographs of spray deposited  $\text{Ag}_2\text{S}$  thin films are recorded using AFM and the resulting micrographs are shown in Fig. 3. Two dimensional micrograph show surfaces with relative uniformity and homogeneity, with the average roughness decreasing from 33.1 nm (S3) to 31.9 nm (S2; see Table 3). Sample S2 exhibits the best morphology covered with spherical shaped grains. On the other hand, When the molarity increases ( $\text{Ag/S} = 0.43$ ), the surface of the films

show uniform clusters with increase in the average roughness value from 37.9 nm (S4) to 43.6 nm (S5). The surface morphology is in good agreement with the composition and crystallinity of the films, which in turn are influenced by the deposition parameters.

### 3.3 Optical studies

The results of transmittance measurements are shown in Fig. 4. It can be seen, all layers have a relatively low transmittance peaks of  $\sim 20\text{--}35\%$  around 1100 nm, and it seems to stabilize for radiation wavelengths below 600 nm. It is noticed that the variations of transmission of the films are consistent with the variations of crystallite size of the layers, Table 3; the greater the crystallite sizes, the higher the optical transmittance of the films as a result of lower photon scattering by the crystallite boundaries. It is also remarkable that a comparison between samples with

**Fig. 3** Fig. 2. AFM 2D and 3D-micrographs of sprayed  $\text{Ag}_2\text{S}$  thin films **a** S1, **b** S2, **c** S3, **d** S4, **e** S5 and **f** S6



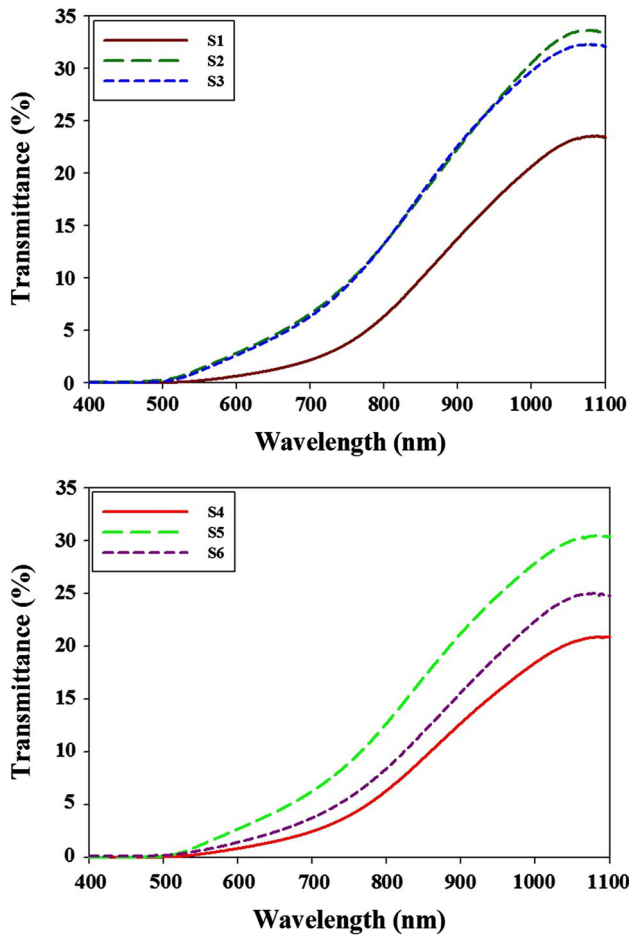


Fig. 4 Optical transmittance spectra of Ag<sub>2</sub>S films

similar substrate growth temperatures shows that the Ag-poor samples (group a) have a higher transmittance than those with higher silver concentrations (group b). This could be due to their lower conductivity, as discussed in Sect. 3.4.

According to the reflectance spectra of the samples, as shown in Fig. 5, with increasing substrate temperature in these two groups, although S2 and S4 samples (prepared at T<sub>s</sub> = 260 °C) have a low (~5–17%) reflectivity in the visible and infrared range (400–1100 nm), it rises to about 30 % in these wavelength region.

The absorption coefficient, α, can be calculated using the formula [15]:

$$\alpha = \frac{1}{d} \ln \left( \frac{(1 - R)^2}{T} \right) \tag{6}$$

where *d*, the thickness of the layers are listed in Table 4. The calculated absorption coefficients in these samples are shown in Fig. 6. According to these results in all samples there is a nearly sharp absorption variation around λ ~ 600 nm. This behavior is in agreement with the band

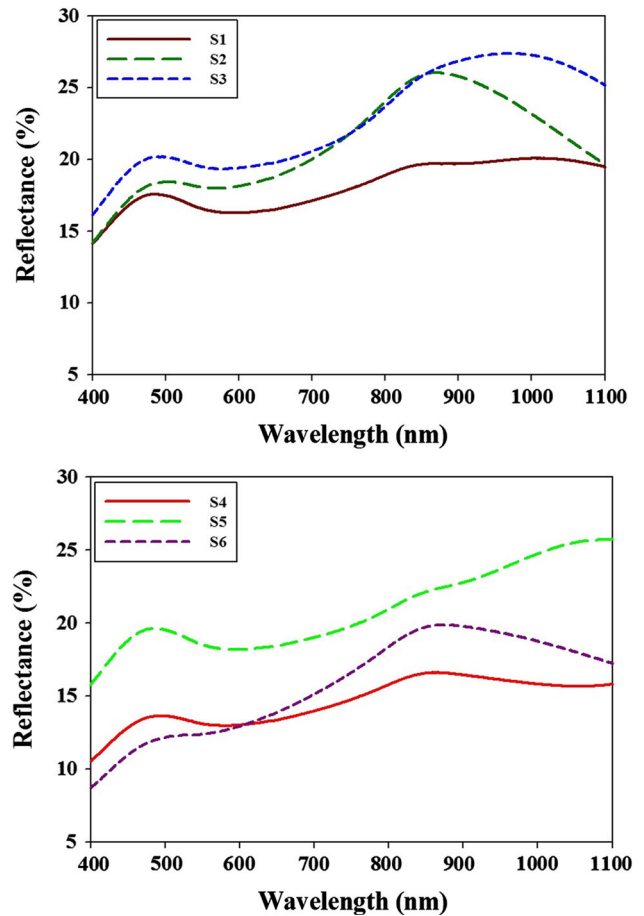


Fig. 5 Optical reflectance spectra of Ag<sub>2</sub>S films

gap calculations given by the plot of (α*hν*)<sup>1/*n*</sup> versus photon energy, *hν*, for interband transitions [16]:

$$(\alpha h\nu)^{1/n} = A(h\nu - E_g) \tag{7}$$

where *A* is a constant and the exponent *n* depends on the type of transition, *n* = 1/2 and 2 for direct and indirect transitions, respectively. The presence of a straight line in the high energy photon range confirms that the involved

Table 4 The thickness, direct band gap and Urbach energy values in the two group samples

Sample	<i>d</i> (nm)	<i>E<sub>g</sub></i> (eV)	<i>E<sub>0</sub></i> (eV)
Group (a) (Ag:S = 0.33)			
S1	210	2.17	0.42
S2	190	2.15	0.37
S3	200	2.22	0.32
Group (b) (Ag:S = 0.43)			
S4	220	2.12	0.51
S5	195	2.23	0.39
S6	205	2.01	0.47

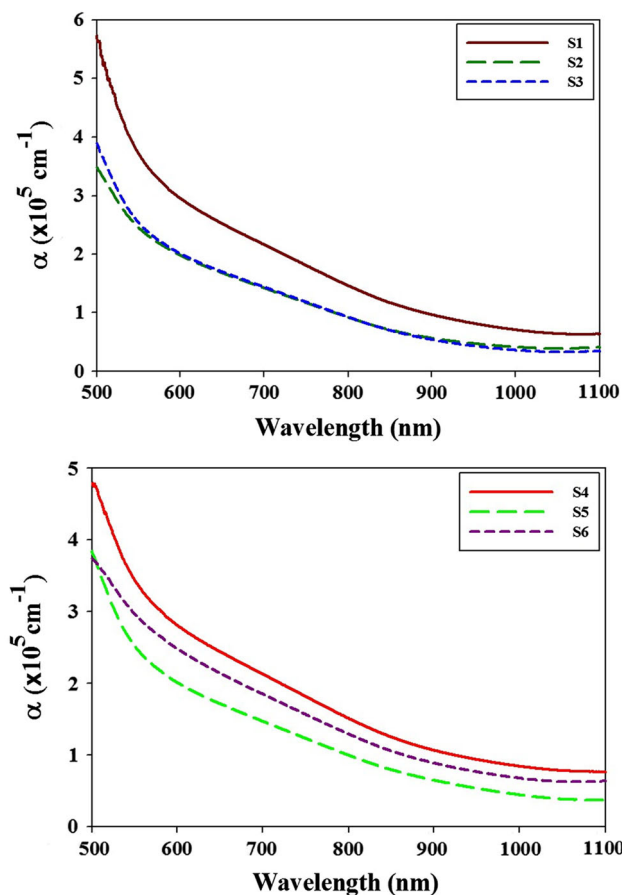


**Fig. 6** The variations of absorption coefficient versus wavelength in various samples

optical transitions are occurred directly across the band gap of the material. This direct band gap could be determined by extrapolating the straight portion to the energy axis, i.e.  $(\alpha h\nu)^2 = 0$ , Fig. 7, and their values are presented in Table 4. As it is apparent in various samples it varies between 2.01 and 2.23 eV. These are in agreement with the result reported for  $\text{Ag}_2\text{S}$  thin film grown by SILAR method [2]. These variations could be attributed to two competitive processes, Burstein–Moss effect [17, 18], which tend to increase the band gap as a result of degeneracy effect due to high carrier concentration in the conduction band (Sect. 3.4); and the presence of wide band tails in the band gap, described in the following, which tend to decrease the efficient band gap of the material.

Although in direct band gap single crystal semiconductors a clear sharp band edges are expected, in non-stoichiometric polycrystalline materials, containing various crystalline defects, the presence of a distributed localized states in the forbidden band gap, forming a band tail, is a possible expectation. Here to estimate the width of the band tail ( $E_0$ ) in  $\text{Ag}_2\text{S}$  layers with expected relatively high crystal defects, we have used Pankove's expression [19]:

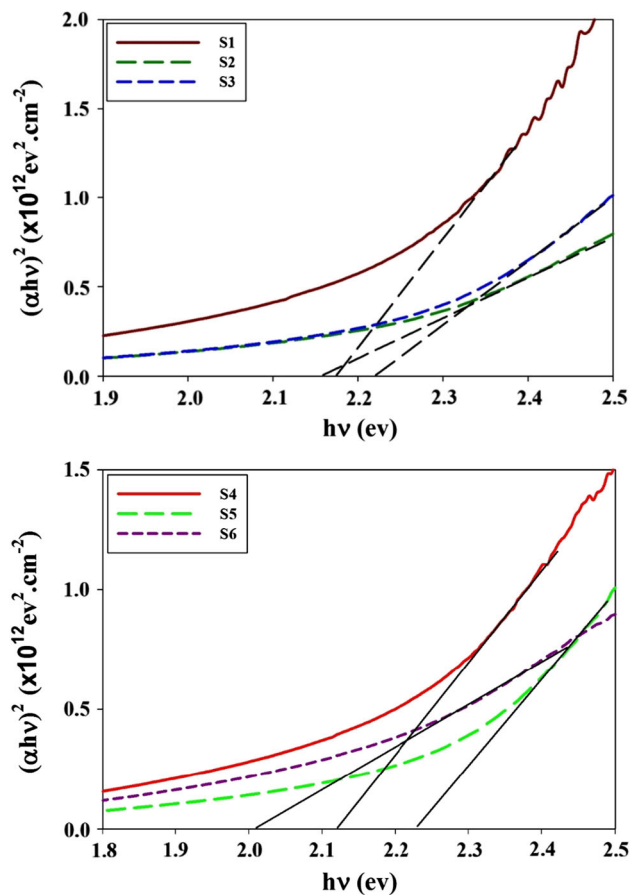


**Fig. 7** The detail analysis for the effective optical band gap determinations in our samples

$$\alpha = BE_0^{3/2} \exp\left(\frac{h\nu}{E_0}\right) \quad (8)$$

where  $B$  is a constant. The empirical parameter  $E_0$  can be deduced from the inverse slope in the semi-logarithm plot of  $\alpha$  against photon energy ( $h\nu$ ) in the tail region. The results are listed in Table 4. A glance on Table 4 shows that: (a) in each group, the  $E_0$  values of the films has decreased as the substrate temperature has increased; (b) the silver-rich samples (group b) have bigger width of the band tails than the poor ones (group a). The decrease of  $E_g$  in this case is connected with the disorder of material caused by variation in the stoichiometry of the material. This leads to redistribution of states from band to tail thus allowing a greater number of possible band to tail and tail to tail transitions. Also, these broad band tails ( $\sim 320$ – $510$  meV) could be a reasonable explanation for the relatively high absorption coefficient in the low photon energy range in the samples (Fig. 6).

### 3.4 Electrical studies

The effect of substrate temperature and Ag:S molar ratio on the electrical properties of the samples were evaluated by

Hall effect and resistivity measurements. Through the Hall data acquisitions we found out that all the studied samples exhibited n-type conductivity, well-matched with other reports [8, 20–22]. The room temperature variations of carrier density ( $n$ ) and resistivity ( $\rho$ ) against the sample numbers (and/or substrate temperature of the samples) are shown in Fig. 8a, b, and their values are given in Table 5. It is noticed that: (1) while the substrate temperature of group (a) samples increases, the electron density gradually changes from  $2.75 \times 10^{14} \text{ cm}^{-3}$  in S1 to  $1.33 \times 10^{14} \text{ cm}^{-3}$  in S2 and then to  $4.05 \times 10^{14} \text{ cm}^{-3}$  in S3; in group (b) it increases from  $3.24 \times 10^{13}$  to about  $3.07 \times 10^{14}$  in S4–S6, respectively. The exact reason for this behavior of ‘ $n$ ’ is not known but this could be understood as follows. It is a well-known fact that the various factors, such as crystallinity, morphology, roughness, porosity, stress, composition, film-substrate interface, etc., play a crucial role in determining the electrical properties of the films. Hence, the variation in the electrical parameters of the films reported in the present study, with respect to substrate temperature and Ag to S molar ratio, can be attributed to the difference in their structural properties as examined by FESEM and XRD. (2) It also should be mentioned that in these two group when substrate temperature increases, the values of resistivity

**Table 5** The resistivity, carrier density and Seebeck coefficient values of Ag<sub>2</sub>S films

Sample	Resistivity ( $\Omega \text{ cm}$ )	Carrier density ( $\times 10^{14} \text{ cm}^{-3}$ )	Seebeck coefficient at 400 K ( $\mu\text{V/K}$ )
Group (a) (Ag:S = 0.33)			
S1	66.15	2.75	–30
S2	11.77	1.33	–117
S3	2.44	4.05	–198
Group (b) (Ag:S = 0.43)			
S4	28.55	0.324	–50
S5	7.17	1.95	–112
S6	7.12	3.07	–194

decreases. These variations of resistivity are consistent with the variations of reflectance of the layers (Fig. 5); the greater the resistivity, the lower the optical reflectance in relation with their poor/rich metallic-like behavior.

### 3.5 Thermoelectrical studies

The variations of Seebeck coefficients as a function of temperature are shown in Fig. 9. Also, Seebeck coefficients

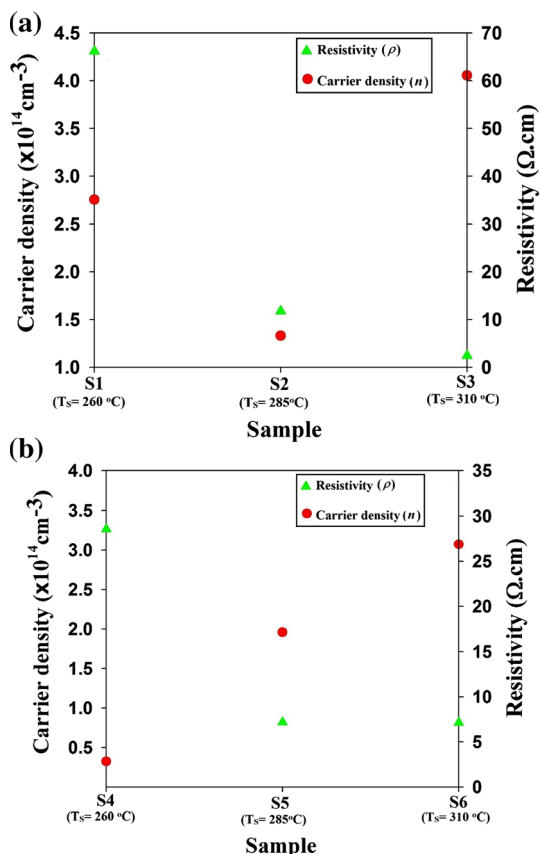


**Fig. 8** Variations of resistivity ( $\rho$ ) and electron density ( $n$ ) in the two group samples

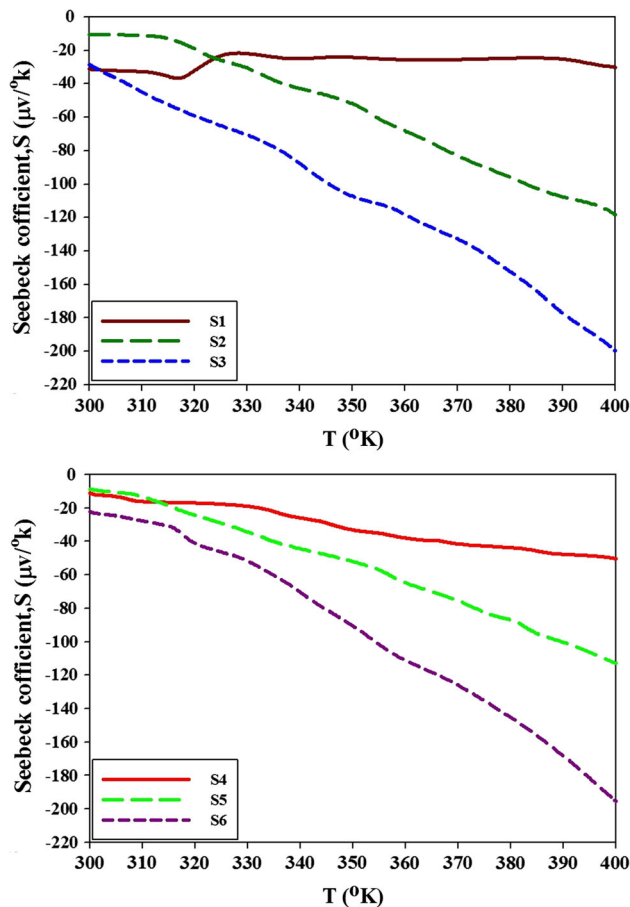


**Fig. 9** Seebeck coefficient versus temperature for Ag<sub>2</sub>S thin films



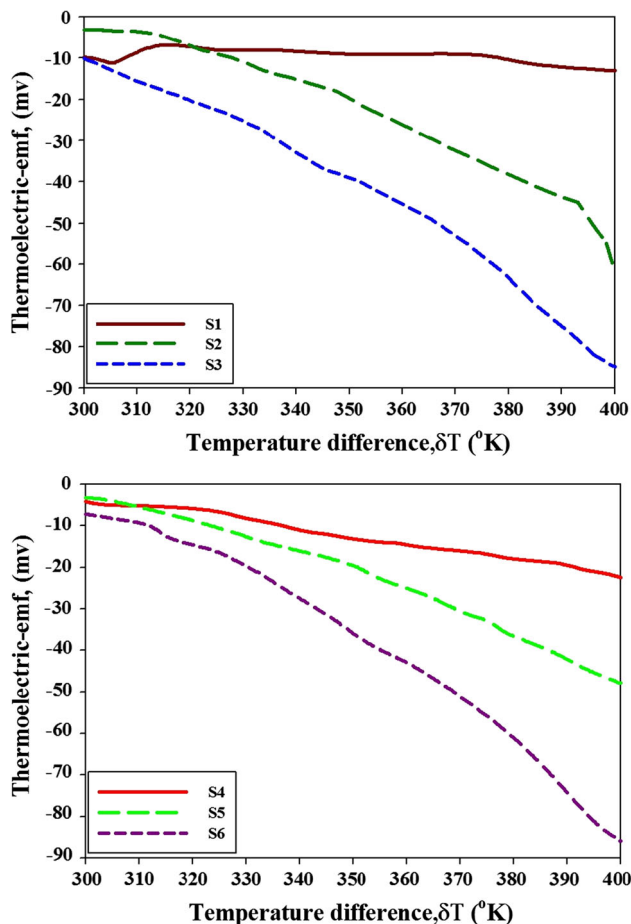


**Fig. 10** Thermoelectric emf versus temperature difference for the studied samples

at  $T = 400$  K are reported in Table 5. Variation of Seebeck coefficient at low temperatures is slow, which increases with linear behavior with increasing temperature higher than 350 K. The maximum Seebeck coefficient of  $-198 \mu\text{V/K}$  (at  $T = 400$  K) was obtained for sample S3 ( $\text{Ag:S} = 0.33$  at.%) at substrate temperature of  $310^\circ\text{C}$ . Figure 10 presents the variation of the thermoelectric emf versus temperature difference ( $\Delta T$ ) between the hot and cold sides for  $\text{Ag}_2\text{S}$  thin films. It is seen that the thermoelectric emf exhibits a linear trend especially for temperature differences in the 340–400 K range. It also should be mentioned that the highest thermoelectric emf was obtained for samples with highest substrate temperature in two groups (a) and (b). The explanation for increasing thermoelectric behavior is either through increased mobility and/or majority carrier concentration with increasing temperature [23]. Since it is likely that mobility does not increase due to probable thermal scattering, we believe the increased thermoelectric behavior is due to ionization of additional majority carriers in these films.

## 4 Conclusions

$\text{Ag}_2\text{S}$  thin films with different Ag to S molar ratios (0.33 and 0.43) have been deposited onto glass substrates by spray pyrolysis method using an aqueous solutions of silver acetate and thiourea at a substrate temperature of  $260$ – $310^\circ\text{C}$ . XRD, SEM and AFM reveal their structure and morphology. The film shows a single  $\alpha\text{-Ag}_2\text{S}$  phase with good crystallinity and the change preferential orientation from  $(\bar{1}12)$  to  $(\bar{1}03)$  plan with increasing Ag:S molar ratio. Referring to AFM studies, sample S2 with Ag:S = 0.33 at substrate temperature of  $285^\circ\text{C}$  exhibit the best morphology covered with spherical shaped grains; also with increasing The molarity ( $\text{Ag:S} = 0.43$ ), the average roughness value increases from 37.9 to 43.6 nm. Optical absorption study revealed direct transition with band gap energy in the range 2.01–2.23 eV, depending on substrate temperate. All the studied samples have an n-type conductivity with a carrier density of about  $10^{14} \text{cm}^{-3}$  which increases with the increment of the substrate temperature, in good agreement with the variations of the reflectance spectra of the layers. The thermoelectric measurements showed that the maximum Seebeck coefficient was obtained equal to  $-198 \mu\text{V/K}$  (at  $T = 400$  K) for  $\text{Ag}_2\text{S}$  thin films with Ag:S = 0.33 at.% concentration in spray solution.

## References

1. K. Sahraoui, N. Benramdane, M. Khadraoui, R. Miloua, C. Mathieu, *Sens. Transducers* **27**, 319 (2014)
2. U.M. Jadhav, S.R. Gosavi, S.N. Patel, R.S. Patil, *Arch. Phys. Res.* **2**, 27 (2011)
3. M.M. El-Nahass, A.A.M. Farag, E.M. Ibrahim, S. Abd-El-Rahman, *Instrum. Sci. Technol.* **72**, 453 (2004)
4. T. Ben Nasrallah, H. Dlala, M. Amlouk, S. Belgacem, J.C. Bernède, *Synth. Met.* **151**, 225 (2005)
5. R. Boughalmi, A. Boukhachem, I. Gaied, K. Boubaker, M. Bouhafs, M. Amlouk, *Mater. Sci. Semicond. Process.* **16**, 1584 (2013)
6. I.C. Lekshmi, G. Berera, Y. Afsar, G.X. Miao, T. Nagahama, T. Santos, J.S. Moodera, *J. Appl. Phys.* **103**, 093719 (2008)
7. A.N. Rodriguez, M.T.S. Nair, P.K. Nair, *Semicond. Sci. Technol.* **20**, 576 (2005)
8. H.M. Pathan, P.V. Salunkhe, B.R. Sankapal, C.D. Lokhande, *Mater. Chem. Phys.* **72**, 105 (2001)
9. B.R. Sankapal, R.S. Mane, C.D. Lokhande, *Mater. Chem. Phys.* **63**, 226 (2000)
10. M. Chen, Y. Xie, H.Y. Chen, Z.P. Qiao, Y.T. Qian, *J. Colloid Interface Sci.* **237**, 47 (2001)
11. N.N. Abdulzadeh, N.N. Mursakulov, R.G. Ahmedsadeh, TPE-06 3rd International Conference on Technical and Physical Problems in Power Engineering, (2006)
12. A.V. Ditman, I.N. Kulikova, *Fizica Tverdogo Tela* **19**(8), 1397 (1977)
13. M.H. Hebb, *J. Chem. Phys.* **20**, 185 (1952)
14. L.J. Van der Pauw, *Philips Res. Rep.* **13**, 1 (1958)

15. P.K. Manoj, B. Joseph, V.K. Vaidyan, D. Sumangala Devi Amma, *Ceram. Int.* **33**, 273 (2007)
16. M. Bouaziz, M. Amlouk, S. Belgacem, *Thin Solid Films* **517**, 2527 (2009)
17. E. Burstein, *Phys. Rev.* **93**, 632 (1954)
18. T.S. Moss, *Proc. Phys. Soc. Lond. Ser. B* **67**, 775 (1954)
19. J.I. Pankove, *Phys. Rev. A* **140**, 2059 (1965)
20. U.M. Jadhav, S.N. Patel, R.S. Patil, *Res. J. Chem. Sci.* **3**, 69 (2013)
21. P.E. Agbo, P.A. Nwofe, *Int. J. Thin Films Sci. Technol.* **9**, 12 (2015)
22. S. Miyatani, *J. Phys. Soc. Jpn.* **10**, 786 (1955)
23. P.S. Patil, L.D. Kadam, *Appl. Surf. Sci.* **199**, 211 (2002)